Physics in Medicine & Biology

PAPER • OPEN ACCESS

Monte Carlo simulations of out-of-field surface doses due to the electron streaming effect in orthogonal magnetic fields

To cite this article: Victor N Malkov *et al* 2019 *Phys. Med. Biol.* **64** 115029

IOP Publishing Phys. Med. Biol. 64 (2019) 115029 (10pp) https://doi.org/10.1088/1361-6560/ab0aa0

Physics in Medicine & Biology

IPEM Institute of Physics and Engineering in Medicine

OPEN ACCESS

PAPER

Monte Carlo simulations of out-of-field surface doses due to the electron streaming effect in orthogonal magnetic fields

Victor N Malkov, Sara L Hackett, Jochem W H Wolthaus, Bas W Raaymakers and Bram van Asselen

Department of Radiotherapy, University Medical Center Utrecht, Heidelberglaan 100, 3584 CX, Utrecht, The Netherlands

E-mail: victormalkov@gmail.com

Keywords: Monte Carlo, MRgRT, magnetic field, surface dose, out-of-field, MR-linac, EGSnrc

RECEIVED
31 July 2018

REVISED
13 February 2019

ACCEPTED FOR PUBLICATION
26 February 2019

PUBLISHED
5 June 2019

Abstract

The out-of-field surface dose contribution due to backscattered or ejected electrons, focused by the magnetic field, is evaluated in this work. This electron streaming effect (ESE) can contribute to out-of-field skin doses in orthogonal magnetic resonance guided radiation therapy machines.

Using the EGSnrc Monte Carlo package, a phantom is set-up along the central axis of an incident 10×10 cm^2 7 MV FFF photon beam. The phantom exit or entry surface is inclined with respect to the magnetic field, and an out-of-field water panel is positioned 10 cm away from, and centered on, the isocenter. The doses from streaming backscattered or ejected electrons, for either a 0.35 T or 1.5 T magnetic field, are evaluated in the out-of-field water panel for surface inclines of 10, 30, and 45°.

The magnetic field focuses electrons emitted from the inclined phantom. Dose distributions at the surface of the out-of-field water panel are sharper in the 1.5 T magnetic field as compared to 0.35 T. The maximum doses for the 0.35 T simulations are 23.2%, 37.8%, and 39.0% for the respective 10, 30, and 45° simulations. For 1.5 T, for the same angles, the maximum values are 17.1%, 29.8%, and 35.8%. Dose values drop to below 2% within the first 1 cm of the out-of-field water phantom. The phantom thickness is an important variable in the magnitude of the ESE dose.

The ESE can produce large out-of-field skin doses and must be a consideration in treatment planning in the MRgRT work-flow. Treatments often include multiple beams which will serve to spread out the effect, and many beams, such as anterior–posterior, will reduce the skin dose due to the ESE. A 1 cm thick shielding of either a bolus placed on the patient or mounted on the present RF coils would greatly reduce the ESE dose contributions. Further exploration of the capabilities of treatment planning systems to screen for this effect is required.

1. Introduction

The ability to visualize and track the treatment target is a major aim in radiation therapy as it allows for margin reduction and potential improvements in sparing healthy tissues of unnecessary dose. An option for image guided radiation therapy is currently implemented using photon-based imaging systems such as portal imagers and cone beam computed tomography with potential further enhancement using optical imaging to correlate patient motion with acquired images (Jaffray and Siewerdsen 2000, Lee *et al* 2008, Dieterich *et al* 2011). Such systems lack soft tissue contrast and often rely on tracking higher density anatomical features as a surrogate for the tumour position. Magnetic resonance imaging (MRI) provides excellent soft tissue contrast, fast visualization capabilities, and a radiation-free imaging solution. These points are the main motivators for development of combined MRI and radiation delivery systems to provide magnetic resonance guided radiation therapy (MRgRT). In addition to enhanced imaging to improve tumour tracking, fast MRI sequences will permit for real-time adaptive radiation therapies (Kontaxis *et al* 2015, Acharya *et al* 2016, Henke *et al* 2016) and functional MRI may be used to further guide patient treatment.

These complex MRgRT systems are well on their development and production stages. The Viewray MRIdian system (Mutic and Dempsey 2014), which comprises a 0.35 T MRI with orthogonal radiation delivery achieved using a three Co-60 or linac source configuration has been used clinically to provide adaptive treatments since

2014. The Elekta Unity system (Raaymakers *et al* 2004, 2017) also uses a perpendicular magnetic and photon field set-up of a 1.5 T Philips MRI and a 7 MV FFF linac to provide an MRgRT solution. This system is installed internationally as part of the MR-linac consortium, and delivered its first-in-man (Raaymakers *et al* 2017) treatments in 2017 at the University Medical Center Utrecht. The MagnetTx Aurora system (Fallone *et al* 2009) combines a 0.5 T magnetic field with a 6 MV linac to achieve radiation delivery parallel to the magnetic field. Australia's currently experimental 1 T MRI and 6 MV linac machine (Keall *et al* 2014) can deliver its radiation beam in both parallel and perpendicular orientations with respect to the magnetic field.

In addition to ensuring that the imaging and radiation delivery systems function properly when combined, developers and researchers have had to address the effects of the magnetic field on patient dose distributions. Some of the effects on the dose distribution are seen through changes in interface doses, the penumbra profile, and the maximum dose depth (Raaijmakers *et al* 2007, 2008, Oborn *et al* 2012, 2014, Keyvanloo *et al* 2016). In-field surface doses are increased in parallel MRgRT systems due to the focusing of electrons generated in the irradiated air or incoming from the linac head (Keyvanloo *et al* 2012, Oborn *et al* 2012). In orthogonal systems, these same electrons are swept out of the primary field and only electrons generated proximal to the patient can contribute to in-field surface doses (Oborn *et al* 2009). The contribution of escaping electrons to out-of-field doses should be explored in greater detail.

The electrons generated in the air continue along the magnetic field lines and have the potential of striking the patient and contributing to skin toxicity outside the main treatment field. Hackett *et al* (2018), using EBT3 film, measured doses of 5.4% $\pm$ 0.2% of the maximum dose deliverable by the beam in a water phantom at surfaces perpendicular to the magnetic field and positioned 5 cm away from the field edge of a $10 \times 10\,cm^2$ field. Recently, Park *et al* (2018) studied treatment plans produced for accelerated partial breast irradiations with either 0 T or 0.35 T magnetic field orthogonal to the photon beams. The group found that the presence of the magnetic field induced doses as large as 15% of the prescription dose to extend in the air along the magnetic field axis and well outside the main treatment region. These findings are further supported by Yang *et al* (2015) who found doses of 3–6 Gy in the neck, lower jaw, and supraclavicular regions in dose distributions calculated using Geant4 for Tomotherapy head and neck plans (prescription of 70 Gy in 35 fractions) with orthogonal magnetic fields ranging from 0.35 T to 3 T. Such high doses, which appear to be much larger than the magnitude of the effect measured by Hackett *et al* (2018), suggests that electrons, generated in the patient and escaping into the air, spiral along the magnetic field and are capable of striking the patient and contributing to skin dose. To evaluate the origin of these high doses, this issue is investigated in detail here for various magnetic field strengths and phantom geometries.

In this work, the EGSnrc Monte Carlo simulation package is used to evaluate the electron streaming effect (ESE). The ESE encompasses electrons which can backscatter or be ejected along the axis of the main radiation beam away from the patient or phantom surface, as exemplified in figure 1. These electrons will then spiral along the magnetic field lines until they impact a surface which may lie outside the treatment field. The ESE is studied here for various entry and exit surface inclines for 0 T, 0.35 T, and 1.5 T magnetic fields. The depth of penetration of the additional out-of-field surface doses is determined in order to produce recommendations as to how to handle cases where the ESE arises.

2. Methods

The egs_chamber (Wulff *et al* 2008) application of the EGSnrc Monte Carlo code system (Kawrakow *et al* 2011) along with the recently implemented and validated enhanced electric and magnetic field macros (Malkov and Rogers 2016) is used in all simulations. All default code parameters were maintained and electron (ECUT) and photon (PCUT) energy cut-offs were set to 521 keV and 10 keV, respectively. Cross section enhancement is used in all simulations with an enhancement factors of 8 and a regional range rejection method is implemented in the the water phantom to reject electrons which are located more than 1.4 times the continuous slowing down range from the surface. The regional rejection method would ignore a portion of the Bremsstrahlung contributions from electrons inside the water phantom. The lack of impact on simulation outcome of the efficiency improvement techniques is verified by comparing a few test simulations with the techniques turned on or off.

The latest available Elekta (Elekta AB, Stockholm, Sweden) generated phase-space files were used for the 7 MV Unity MR-linac accelerator. The phase-space is for a $10 \times 10\,cm^2$ field size defined at the isocenter, located at 143.5 cm away from the particle source. The particles in the phase-space file are stored at 129.5 cm away from the source. To improve efficiency in the magnetic field simulation, the electrons and positrons from the phase-space file are not simulated as they are unable to reach the scoring regions of interest in the simulation. Test simulations did not produce differences in results between using or excluding the charged particles from the file.

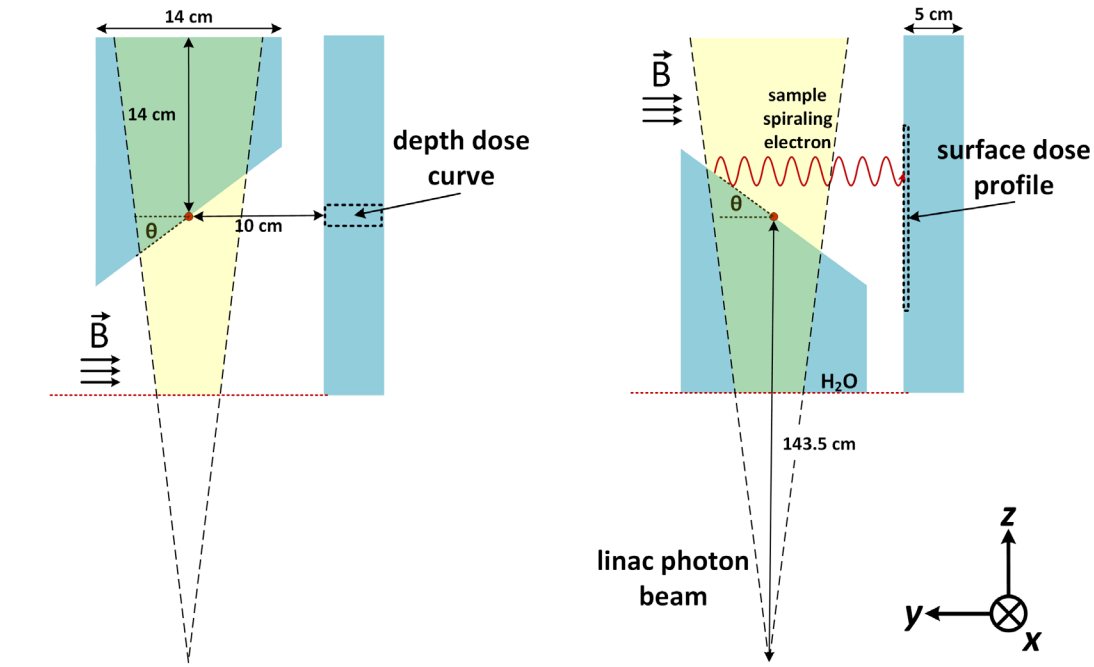

Figure 1. Schematic of the set-up for the (a) entry and (b) exit streaming simulations. The phase-space photon source, scored at 129.5 cm from the source (dashed red line), is incident on the inclined water phantom. The inclined surface of the phantom is always centred at the isocenter (red dot) and the thickness from the base to isocenter is maintained as 14 cm (except for the varying thickness simulations in section 2.3). The magnetic field is directed along the negative *y*-axis. The effect of the magnetic field is shown on a sample electron (sinusoidal red line). In both the entry and exit simulations a depth dose curve and a surface dose profile is scored.

2.1. Entry and exit ESE phantom set-up

To evaluate the electron streaming effect (ESE) a simple geometry is implemented and a schematic can be viewed in figure 1. To determine the ESE contribution to out-of-field doses due to backscattered electrons, the entry streaming phantom is set up with the center of the entry surface positioned at isocenter. The phantom thickness, defined as the distance from the center of the inclined surface to the flat base of the phantom, is 14 cm. The center of the inclined surface is always positioned at the isocenter for the 10, 30, and 45° simulations. The exit streaming phantom is set-up in a similar manner with the inclined surface center always being at isocenter and the same phantom thickness as the entry simulation. The difference is that the entry surface facing the beam is flat and begins at 129.5 cm. In both simulations the magnetic field is oriented in the negative y direction (defined as is ICE1217 machine coordinate system) and is set to either 0, 0.35, or 1.5 T. A water panel with dimensions of 20 cm × 5 cm × 30 cm in the *x*, *y*, and *z* directions, respectively, is positioned 10 cm away from, and centered on, isocenter. In both the entry and exit streaming simulations a depth dose curve and a surface dose profile are determined. All doses are reported as a percentage of the maximum deliverable dose, D_{max}, by the beam. D_{max} is calculated in a separate simulation in a $30 \times 30 \times 30$ cm^3 water phantom with an SSD of 133.5 cm. The maximum dose is determined for each of the simulated magnetic fields by scoring the central axis depth dose curve in voxels with a 0.5×0.5 cm^2 surface area and a thickness of 0.2 cm along the direction of the beam. The depth dose curves in the out-of-field water panel are determined in voxels with a surface of 1 cm × 1 cm along the *x* and *z* directions and 0.1 cm thick segments into the water panel along the *y*-axis. The surface dose profile is calculated in the first 0.1 cm of the water panel in a 40 × 80 pixel region along the *z* and *x* directions, respectively. Each side of the individual pixels of the profile is 0.25 cm.

In these simulations backscattered or ejected electrons would be able to spiral along the magnetic field. This is shown in figure 1 by the red sinusoidal line. Some of the electrons will be able to return to the surface of the water phantom. A portion of the spiralling electrons will be those generated in the air, but this is expected to be a small contribution as compared to the number of electrons emitted from the water phantom. In the work of Raaijmakers *et al* (2005) the phantoms considered were effectively rotated by 90° around the *z*-axis relative to the ones considered here and the impact of the magnetic field on the in-field surface doses was evaluated.

In addition to the simulations with the water phantom as presented in figure 1, the exit streaming phantom was rotated by 90° along the *z*-axis while keeping the out-of-field water panel in the same location. This geometry is similar to that of Raaijmakers *et al* (2005), but the dose outside the primary field is of interest. This rotation

resulted in the angled surface of the water phantom to be inclined along the x-axis instead of along the y-axis as in figure 1. This permitted the analysis of the ESE for exit surface parallel to the magnetic field. Results are presented for 0 T, 0.35 T, and 1.5 T magnetic fields with a 0° slope of the surface, and for a 1.5 T field with a 10° and 45° slope with the water phantom rotated +90° along the z-axis (sloped surface pointing towards the positive x-axis) and with a 45° slope with the water phantom rotated −90° (sloped surface towards the negative x-axis). This set-up corresponds to beams incident on the side of the patient and which may be slightly inclined with respect to the incoming photon beam.

2.2. Effect of distance on the ESE

Once the electrons are backscattered or ejected from the water surface, the magnetic field will reduce lateral scatter of these electrons away from the magnetic field lines. This implies that moving the dose scoring water panel further away from isocenter should not produce large variations in the results (aside from some energy loss and scatter in the air). In the absence of a magnetic field, the out-of-field electron dose contribution would decrease due to scatter, energy loss, and the inverse square law. To evaluate the ESE as a function of distance, the water panel is positioned at 10, 20, and 30 cm away from isocenter. The surface dose profile is evaluated for the exit phantom, as in figure 1, with a 30° incline with a 1.5 T magnetic field at these locations.

2.3. Varying phantom thickness

Since photon fluence is directly correlated with the generated secondary electron fluence, the attenuation of the photon beam produces a decline in the total electron fluence with phantom depth. This indicates that increasing phantom thickness would produce fewer electrons, which would be able to exit the phantom and stream towards the scoring water panel. To evaluate the variation of the ESE doses as a function of phantom thickness, the thickness of the exit water phantom is set to 10, 18, or 26 cm for an incline of 30°. Since the phase-space file begins at 129.5 cm, the center of the inclined exit surface of the water phantom is positioned at 155.5 cm. This allows the inclined exit surface to remain in the same location while the thickness of the phantom is varied and as such the inverse square effects on the photon beam are equal for all of the thickness simulations. The scoring water panel is appropriately shifted such that its center is aligned with the center of the inclined exit surface of the water phantom. The surface dose profiles on the water panel is presented for each thickness.

2.4. ESE for a 2×2 cm^2 field size

Since smaller fields are generally used in intensity modulated radiation treatments, the ESE is evaluated for a 2×2 cm^2 field size defined at isocenter. An Elekta generated phase-space file is also used for these simulation, and the phase-space scoring plane is also at 129.5 cm away from the source. The exit phantom, with the 10, 30, and 45° inclines, as described in section 2.1 is used in these simulations and only the 0.35 T and 1.5 T magnetic field simulations are presented. The normalizing D_{max} is appropriately recalculated for these magnetic fields using the smaller field size.

3. Results and discussion

Below the results for the various studies of this work are presented. Both surface dose profiles and depth dose curves in the out-of-field water panel are shown. The reader's attention is drawn to the variations in the scale used for the various figures of the surface dose profiles. The colour scale is inter-comparable between panels of each figure, but not between different figures. In all of the surface dose profile panels the photon beam is incident from the negative z-axis.

3.1. Entry backscatter ESE doses

Figure 2 provides the water dose panel surface profiles for the entry backscatter phantom presented in section 2.1. The results are given for 0, 0.35, and 1.5 T with 10, 30, and 45° incline for each magnetic field. The 0 T results show little out-of-field backscatter dose. The maximum effect for the 0 T case is on the order of a few percent at most. The introduction of the magnetic field demonstrates the ESE as the electrons are focused by the magnetic field and the inclined surface area of the 10×10 cm^2 beam is projected onto the side water panel. The 1.5 T magnetic field, due to the smaller gyroradius, produces a sharper dose profile than the 0.35 T case. The largest ESE dose for the backscattered electrons is seen for the 45° surface angle with maximum isodose curves of roughly 5.0% and 8.5% for the 0.35 T and 1.5 T magnetic fields, respectively.

In figure 3 the depth dose curves in the side water panel for the entry streaming calculation are presented. In all cases, within approximately the first 0.5 cm of the water phantom all the surface angle simulations converge to a roughly equivalent out-of-field dose. The sharp drop-off for the magnetic field simulations is anticipated since the electrons striking the panel would quickly lose their energy near the surface of the panel. These results are consistent with the measurements of Hackett *et al* (2018) who saw that the air born electrons which spiral along

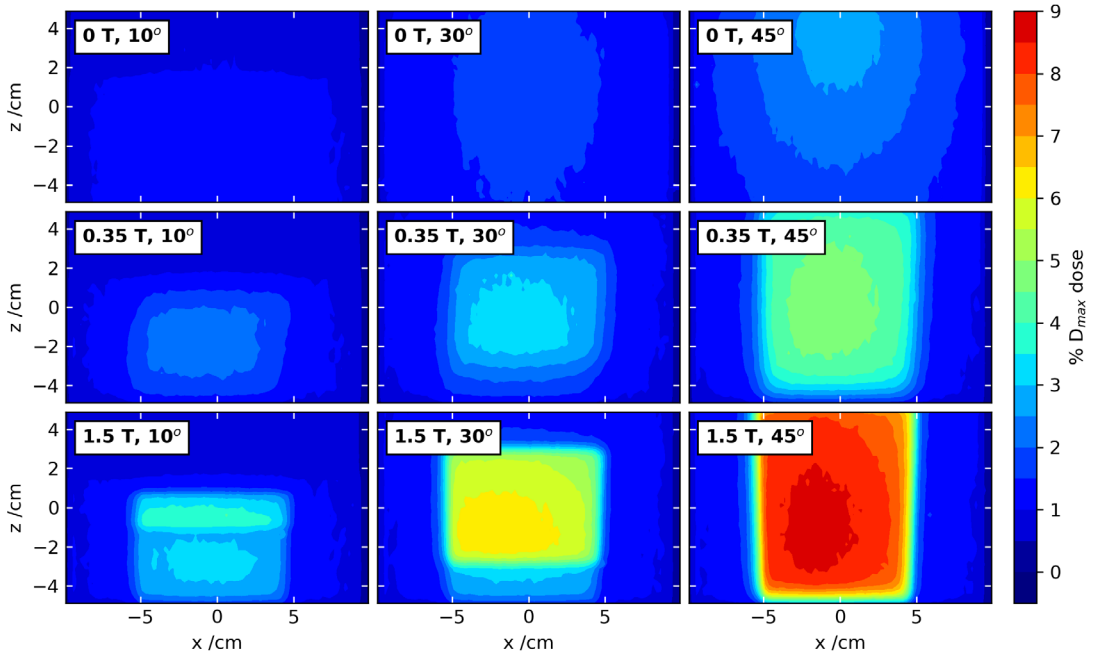

Figure 2. Surface dose profiles for the entry simulation shown in figure 1 with a 10, 30, and 45° inclines for 0, 0.35, and 1.5 T .

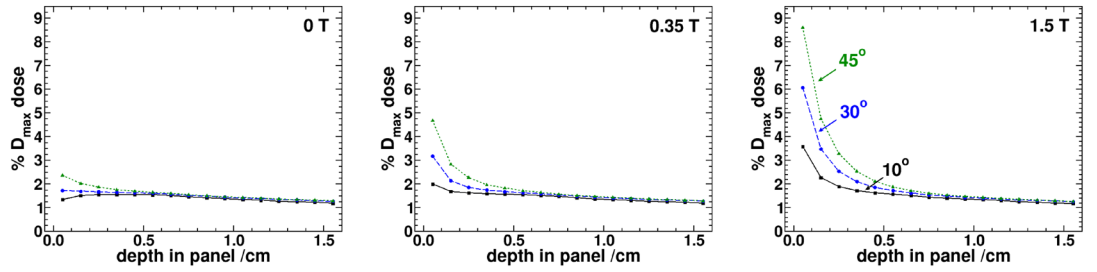

Figure 3. Depth dose curves for the entry simulation shown in figure 1 with a 10, 30, or 45° incline for 0, 0.35, and 1.5 T. Each point represents the average dose in a 1 mm thick region into the phantom.

the magnetic field contribute to out-of-field dose increases only in the first few millimetres of the measurement panel.

3.2. Exit ejected ESE doses

In figure 4 the exit streaming simulation results are presented. The 0 T simulations show a fairly diffused distribution with all values within 9%, with the higher doses appearing in the upper region of the 45° simulation results (these values are difficult to observe in figure 4 due the colour scale). Again the presence of a magnetic field allows the projection of ejected electrons from the surface onto the side water panel, and the stronger magnetic field produces a sharper dose profile due to the smaller radius of curvature of the electron trajectories. The maximum doses for the 0.35 T simulations are 23.2%, 37.8%, and 39.0% for the respective 10, 30, and 45° simulations (each value carries an absolute uncertainty of 0.2%). For the 1.5 T simulations for the same angles the maximum values are 17.1%, 29.8%, and 35.8% (absolute uncertainty of 0.2%). Perhaps somewhat counter-intuitively, the lower 0.35 T magnetic field produces a larger maximum dose value as compared to 1.5 T. Though this is not the case in the entry simulation in section 3.1 as it is linked to the energy and the backscatter direction distribution of the electrons. In the exit simulations in this section, both the 0.35 and 1.5 T magnetic fields produce the ESE, but the lower magnetic field induces a larger radius of curvature of the electron trajectories than the 1.5 T field. This allows more electrons to escape the surface of the inclined phantom, and stream towards the out-of-field water panel. As is seen in section 3.5 below, the lower magnetic field does not always produce an overall larger maximum ESE dose.

Particularly in the 1.5 T simulations and most distinct for the 45° phantom, there is a dose gradient along the z-axis of the surface dose profiles. This is attributed to two effects and both have to do with the incline of the exit surface. The first is the inverse square effect which produces a difference in the photon fluence between the lower

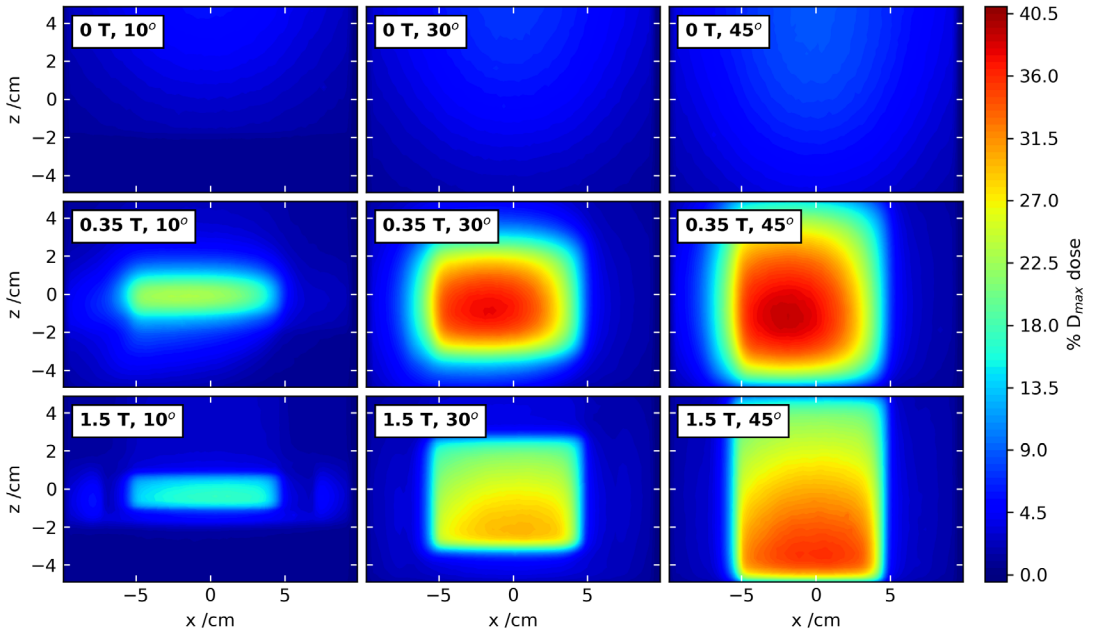

Figure 4. Surface dose profiles for the exit simulation shown in figure 1 with a 10, 30, and 45° inclines for 0, 0.35, and 1.5 T .

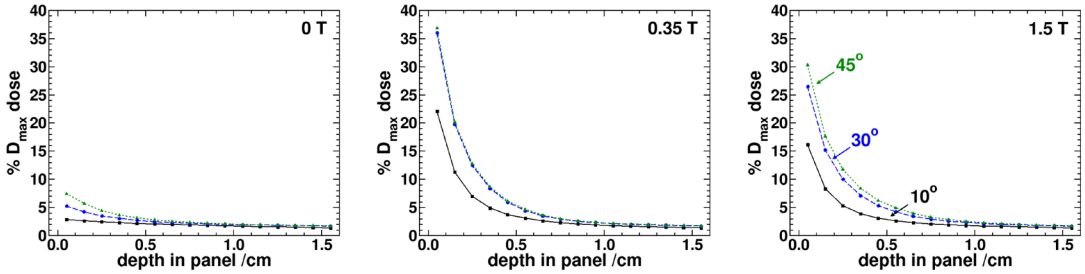

Figure 5. Depth dose curves for the exit simulation shown in figure 1 with a 10, 30, or 45° incline for 0, 0.35, and 1.5 T. Each point represents the average dose in a 1 mm thick region into the phantom.

and upper edge of the inclined phantom. The second effect here is the attenuation of the photon beam which increases from the lower to the upper edge of the water phantom. Combined, these two effects produce a gradient in the overall electron fluence along the surface of the inclined phantom.

Figure 5 provides the depth dose curves in the side water panel for the exit ESE simulations. Similarly to the entry simulations, there is a sharp fall-off in the dose with depth. In these simulations a rough convergence between the different inclines and a drop below 2% in the magnetic field simulations is attained at a depth of about 1 cm into the water phantom.

Simulations with the water phantom rotated by 90° along the z-axis are shown in figure 6. The 0° simulations correspond to the streaming of ejected electrons along a flat surface. In this case, again, the 0 T results show little out-of-field contribution as compared to the 0.35 T and 1.5 T results. For the 0.35 T simulations there is a roughly 10% contribution within the region of the primary beam near the water phantom exit surface, while, for 1.5 T, in the same region the effect is approximately 5%. This is due to the higher magnetic field causing more of the high energy electrons to return to the surface of the water phantom, while the 0.35 T magnetic field leads to streaming of electrons along spirals with much larger radii which allows these electrons to travel beyond the extents of the water phantom. Because of this larger gyroradius the region of increased out-of-field dose is more diffused for the 0.35 T field. At the edges of the water phantom (at $x = \pm 7$ cm) electrons escaping are more likely to not meet a surface when completing a rotation in the magnetic field due to the geometry of the phantom, and this leads to small localized hot spots which are more pronounced in the 1.5 T field. For the 1.5 T simulations, increasing the slope to 10° does not produce a notable change in the distribution, while in the 45° slope with the $+90°$ rotation case there a reduction in the out-of-field dose. Looking at the same 45° slope, but with a $-90°$ rotation, there an increasing the out-of-field contribution as compared to the 0° simulation. This difference in the 45° slope calculations is due to the electrons rotating counter-clockwise, as viewed from the out-of-field scoring panel,

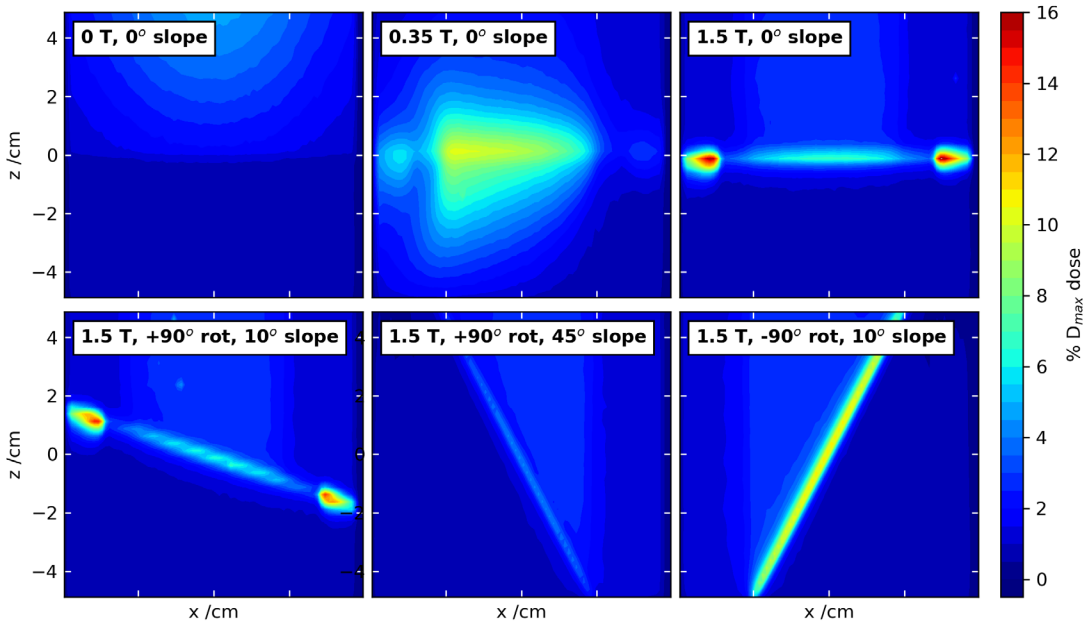

Figure 6. Surface dose profiles with the water phantom surface sloped by 0° for 0 T, 0.35 T, and 1.5 T, and, for 1.5 T, by 10° and 45° for a positive 90° rotation and 45° for a negative 90° rotation along the *z*-axis.

which causes more electrons to return to the water phantom surface in the +90° rotation orientation while more electron are able to escape in the −90° rotation simulation. The majority of the out-field dose is confined to about 1.5 cm and 0.5 cm away from the surface of the water phantom for the 0.35 T and 1.5 T magnetic fields, respectively.

3.3. Effect of distance on the ESE

Figure 7 presents the surface dose profiles for 30° and 1.5 T magnetic field with the panel positioned at 10, 20, or 30 cm away from isocenter. The maximum dose values on these profiles are 29.8%, 26.5%, and 24.1% (absolute uncertainty of 0.2%) for the 10, 20, and 30 cm positions, respectively. As anticipated, moving the panel further away does not produce large variation in the surface dose profiles on the ESE out-of-field dose. Therefore, even if the treatment area is farther away from the patient there could be a sufficient number of electrons, which would be able to reach the patient and could contribute to skin dose if there are no obstructions along the path of the electrons.

In addition to variation of the ESE dose due to the water panel position, because of the inverse square law the distance of the entry or exit surface with respect to the source contributes to the magnitude of the ESE. The center of the slanted surface in the previous sections is positioned at the isocenter. Clinically, it is more likely that the isocenter is positioned at depth within the patient. The 30° simulations are repeated with the slanted phantom shifted 5 cm towards or away for the entry or exit simulations, respectively. In this way, the isocenter is within the phantom in both simulations. The maximum dose in the water panel, which is moved in unison with the slanted phantom, changes by +6.2% ± 0.4% and −8.2% ± 0.4% from the not shifted result for the respective shifted entry and exit simulations. These changes are comparable to the expected inverse square law effect which would predict an approximately +7.4% and −6.4% change for the corresponding entry and exit simulations, and the differences are likely due to slight variations in photon scatter contributions.

3.4. Varying phantom thickness

The simulations with varying water phantom thickness for the 30° and 1.5 T magnetic field show that the maximum values on the surface profiles are 27.8%, 22.2%, and 17.8% (absolute uncertainty of 0.2%) for the 10, 18, and 26 cm phantom thickness, respectively. The variation in the maximum phantom surface dose is more pronounced here than for the panel position variation. This is expected as the exit ESE dose is dependent on the percent depth dose value in the water phantom for each of the depths. The 10 cm thickness maximum value is lower than the 14 cm thickness value reported above, and this is due to the phantom having to be shifted farther away from the beam to accommodate for the extra thickness required and the phase-space scoring plane being defined at 129.5 cm.

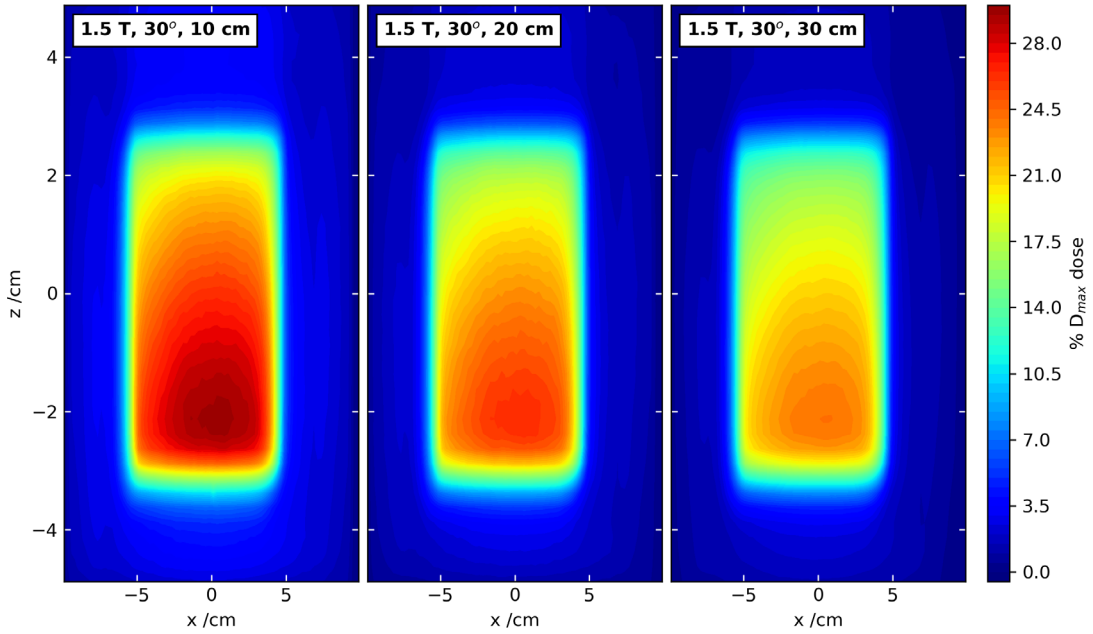

Figure 7. Exit streaming dose simulations for a 30° incline with a 1.5 T magnetic field and with the surface of the out-of-field water panel positioned at 10, 20, and 30 cm distance away from isocenter.

3.5. ESE for a $2 \times 2\,cm^2$ field size

In figure 8 the dose profiles for the 0.35 T and 1.5 T magnetic fields with the 10, 30 and 45° inclines with a $2 \times 2\,cm^2$ incident photon beam are presented. The 1.5 T magnetic field produces a much greater focusing effect as compared to the blurred dose distributions of the 0.35 T results. The maximum dose values for the 0.35 T simulations are 4.0% ± 0.1%, 10.72% ± 0.03%, and 14.78% ± 0.05% for the 10, 30, and 45° simulations, respectively. For the 1.5 T, for the same angles, the maximum values are 8.51% ± 0.03%, 20.87% ± 0.06%, and 25.98% ± 0.08%.

The maximum values of the 1.5 T simulations in figure 8 are larger than the 0.35 T field results. This is due to the lateral electron equilibrium, depicted in figure 9 in which the point-of-view of the out-of-field water slab is taken in order to demonstrate the curvature of the incoming streaming electrons in the exit phantom simulation. The impact of a large, FS_L, and small, FS_S, field size, as compared to the electron curvature, on the establishment of a lateral electron equilibrium is shown. For a sufficiently large field size, electrons which exit the area of interest, AOI, can be compensated by electrons which are generated upstream along the *x*-axis and curve into the AOI. As the field size is reduced, the availability of these compensating electrons is diminished and the same electron fluence as in the larger field size cannot be maintained in the AOI. This lateral electron equilibrium in the streaming electron fluence is dependent, aside from the field size, on the radius of curvature and, as such, on the magnitude of the magnetic field, electron kinetic energy, and electron's direction of motion.

4. Conclusion

The results presented here demonstrate that the electron streaming effect (ESE), in which the magnetic field focuses backscattered or ejected electron from a phantom to travel along the magnetic field lines, can produce doses as high as 39.0% ± 0.2% (45° exit streaming, 0.35 T, $10 \times 10\,cm^2$) of the maximum deliverable dose by the photon beam in a large water phantom. This effect has direct consequences on out-of-field skin doses and should be considered during planning of MRgRT treatments. The effect is highly dependent on the angle of the treatment surface with respect to the magnetic field, and certain treatment sites (such as breast) should be approached with greater caution in light of this effect. Conversely, treatment volumes for which the patient surface is roughly parallel to the magnetic field will see little ESE doses and those inclined towards inconsequential regions will have electrons streamed away from the patient and not contribute to out-of-field skin dose. Lower magnetic fields produce a more diffuse out-of-field dose distribution, and the magnitude of the maximum ESE dose for a given magnetic field depends highly on the photon field size. Further, although the distance away from the treatment site does not produce large variation in the ESE doses, the thickness of the treatment region does play an important role in the magnitude of the effect. Thicker regions will produce greater attenuation of the photon beam, and fewer electrons can be focused by the magnetic field. However, this does mean that thinner or less attenuating regions (e.g. thorax) will result in a relative increase in streaming electrons and higher ESE doses.

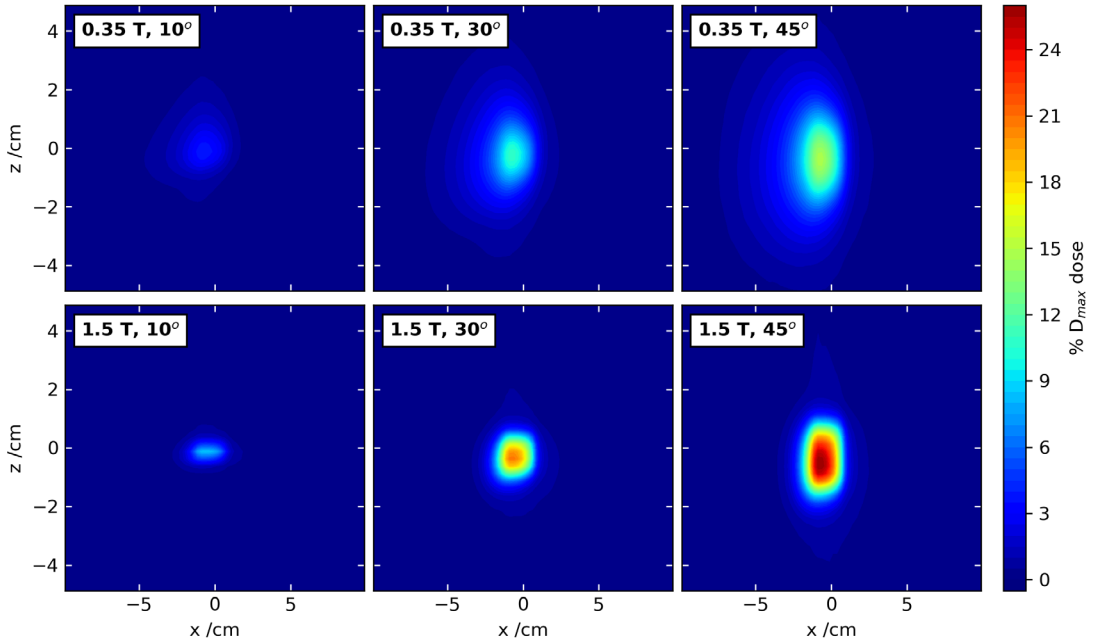

Figure 8. Exit streaming dose simulations for 10, 30, and 45° inclines with a 0.35 or 1.5 T magnetic field for a 2 cm × 2 cm photon beam.

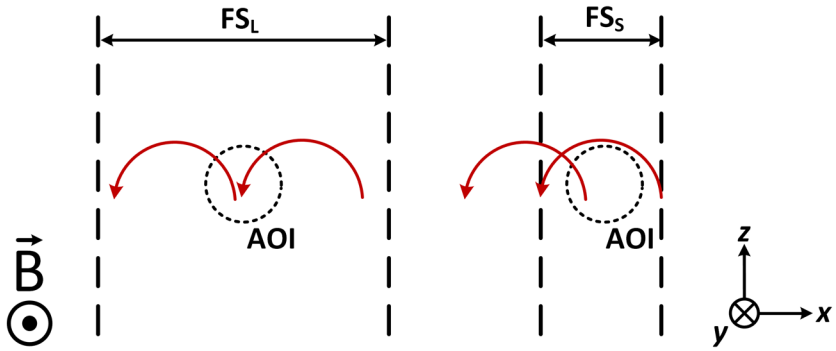

Figure 9. Point of view of the out-of-field water slab (along the negative *y*-axis) of the exit phantom streaming electrons. Sample electron tracks are depicted by the curved arrows. For the larger field size, FS_L, electrons exiting the area of interest, AOI, are compensated by electrons curving into the region from further up the *x*-axis. In the case of the smaller field size, FS_S, it is not possible to set up a lateral electron equilibrium due to unavailability of similar electrons which can curve into the AOI to maintain the electron fluence.

The calculations presented in this work do not reflect a clinical treatment plan. Most often, multiple beams are used in treatments and part of these beam will be directed anterior–posterior. Such beams will contribute far less to the ESE dose since only backscattered electrons will participate in the effect. As shown in this work, the backscatter ESE contribution in a 1.5 T magnetic field with a 30° inclined surface is within 7% of the maximum deliverable dose by the beam. The percentage values quoted in this work are for a single beam and do not directly represent a percentage of the prescribed dose. Since the ESE is a predictable effect, having knowledge of the body contour and the beam direction, it is possible to anticipate cases in which the out-of-field doses may be an issue.

In cases where the ESE dose cannot be fully mitigated a bolus or some sort of shield would be required. As proposed by Park *et al* (2018) and supported by the simulations in this work, the thickness of the bolus should be at least 1 cm to ensure proper shielding from the incoming electrons. Although currently not in development, any upgrades to MRgRT system which include higher energy beams would likely need to consider thicker shielding. An additional solution may be mounting a more rigid shielding on the RF-coils which are already present at the treatment site in MRgRT machines. Such a shielding system would not only be able to block ESE doses but also some of the dose contributions from electrons generated in the air (Hackett *et al* 2018).

Further attention is certainly required into this issue in order to evaluate in which cases shielding should be considered. Treatment planning systems (TPS) need to be tested to ensure that they are able to fully describe this effect and whether users need to indicate additional regions in which the TPS should perform more detailed

calculations. The ability to see this effect in the TPS would permit more thorough screening of patients and determination of the magnitude of the ESE in specific clinical cases.

Acknowledgments

The authors would like to thank David W O Rogers and the Carleton Laboratory for Radiotherapy Physics for granting the use of the Carleton Physics Department CPU computing cluster. This work was partially funded by EURAMET through EMPIR grant 15HLT08 MRgRT.

References

Acharya S *et al* 2016 Online magnetic resonance image guided adaptive radiation therapy: first clinical applications *Int. J. Radiat. Oncol. Biol. Phys.* **94** 394–403

Fallone B G, Murray B, Rathee S, Stanescu T, Steciw S, Vidakovic S, Blosser E and Tymofichuk D 2009 First MR images obtained during megavoltage photon irradiation from a prototype integrated linac-MR system *Med. Phys.* **36** 2084–8

Hackett S, van Asselen B, Wolthaus J, Bluemink J, Ishakoglu K, Kok J, Lagendijk J and Raaymakers B 2018 Spiraling contaminant electrons increase doses to surfaces outside the photon beam of an MRI-linac with a perpendicular magnetic field *Phys. Med. Biol.* **63** 095001

Henke L *et al* 2016 Simulated online adaptive magnetic resonance–guided stereotactic body radiation therapy for the treatment of oligometastatic disease of the abdomen and central thorax: characterization of potential advantages *Int. J. Radiat. Oncol. Biol. Phys.* **96** 1078–86

Jaffray D and Siewerdsen J 2000 Cone-beam computed tomography with a flat-panel imager: initial performance characterization *Med. Phys.* **27** 1311–23

Kawrakow I, Mainegra-Hing E, Rogers D W O, Tessier F and Walters B R B 2019 The EGSnrc code system: Monte Carlo simulation of electron and photon transport *NRC Technical Report* PIRS-701 (Ottawa, Canada: National Research Council Canada) (https://nrc-cnrc.github.io/EGSnrc/doc/pirs701-egsnrc.pdf)

Keall P J *et al* 2014 The australian magnetic resonance imaging–linac program *Semin. Radiat. Oncol.* **24** 203–6

Keyvanloo A, Burke B, Aubin J S, Baillie D, Wachowicz K, Warkentin B, Steciw S and Fallone B 2016 Minimal skin dose increase in longitudinal rotating biplanar linac-MR systems: examination of radiation energy and flattening filter design *Phys. Med. Biol.* **61** 3527

Keyvanloo A, Burke B, Warkentin B, Tadic T, Rathee S, Kirkby C, Santos D M and Fallone B G 2012 Skin dose in longitudinal and transverse linac-MRIs using Monte Carlo and realistic 3D MRI field models *Med. Phys.* **39** 6509–21

Kontaxis C, Bol G, Lagendijk J and Raaymakers B 2015 A new methodology for inter-and intrafraction plan adaptation for the MR-linac *Phys. Med. Biol.* **60** 7485

Lee S W, Jin J Y, Guan H, Martin F, Kim J H and Yin F F 2008 Clinical assessment and characterization of a dual-tube kilovoltage x-ray localization system in the radiotherapy treatment room *J. Appl. Clin. Med. Phys.* **9** 1–15

Malkov V N and Rogers D W O 2016 Charged particle transport in magnetic fields in EGSnrc *Med. Phys.* **43** 4447–58

Mutic S and Dempsey J F 2014 The ViewRay system: magnetic resonance-guided and controlled radiotherapy *Semin. Radiat. Oncol.* **24** 196–9

Oborn B M, Kolling S, Metcalfe P E, Crozier S, Litzenberg D W and Keall P J 2014 Electron contamination modeling and reduction in a 1 T open bore inline MRI-linac system *Med. Phys.* **41** 051708

Oborn B M, Metcalfe P E, Butson M J and Rosenfeld A B 2009 High resolution entry and exit Monte Carlo dose calculations from a linear accelerator 6 MV beam under the influence of transverse magnetic fields *Med. Phys.* **36** 3549–59

Oborn B M, Metcalfe P E, Butson M J, Rosenfeld A B and Keall P J 2012 Electron contamination modeling and skin dose in 6 MV longitudinal field MRIgRT: impact of the MRI and MRI fringe field *Med. Phys.* **39** 874–90

Park J M, Shin K H, Kim J I, Park S Y, Jeon S H, Choi N, Kim J H and Wu H G 2018 Air-electron stream interactions during magnetic resonance IgRT *Strahlentherapie Onkol.* **194** 50–9

Raaijmakers A J E, Raaymakers B W and Lagendijk J J W 2005 Integrating a MRI scanner with a 6 MV radiotherapy accelerator: dose increase at tissue-air interfaces in a lateral magnetic field due to returning electrons *Phys. Med. Biol.* **50** 1363–76

Raaijmakers A J E, Raaymakers B W and Lagendijk J J W 2007 Experimental verification of magnetic field dose effects for the MRI-accelerator *Phys. Med. Biol.* **52** 4283–91

Raaijmakers A J E, Raaymakers B W and Lagendijk J J W 2008 Magnetic-field-induced dose effects in MR-guided radiotherapy systems: dependence on the magnetic field strength *Phys. Med. Biol.* **53** 909–23

Raaymakers B *et al* 2017 First patients treated with a 1.5 T MRI-linac: clinical proof of concept of a high-precision, high-field MRI guided radiotherapy treatment *Phys. Med. Biol.* **62** L41

Raaymakers B W, Raaijmakers A J E, Kotte A N T J, Jette D and Lagendijk J J W 2004 Integrating a MRI scanner with a 6 MV radiotherapy accelerator: dose deposition in a transverse magnetic field *Phys. Med. Biol.* **49** 4109–18

Dieterich S *et al* 2011 Report of AAPM TG 135: quality assurance for robotic radiosurgery *Med. Phys.* **38** 2914–36

Wulff J, Zink K and Kawrakow I 2008 Efficiency improvements for ion chamber calculations in high energy photon beams *Med. Phys.* **35** 1328–36

Yang Y, Geurts M, Smilowitz J, Sterpin E and Bednarz B 2015 Monte carlo simulations of patient dose perturbations in rotational-type radiotherapy due to a transverse magnetic field: a tomotherapy investigation *Med. Phys.* **42** 715–25